文章编号:1004-5929(2014)04-0398-08

基于内嵌旋转银纳米方块圆形纳米腔的折射率传感器

曹 威[1],秦 艳[1],张中月[1,2*]

(1. 西南大学物理科学与技术学院,重庆 400715;2. 陕西师范大学物理学与信息技术学院,西安 710062)

摘 要:本文设计了一个基于内嵌可旋转银纳米方块圆形纳米腔的金属-介质-金属波导滤波器,并用时域有限差分算法进行了表征。由于旋转的银纳米方块破坏了圆形纳米腔原有的对称稳态磁场分布,因而产生了一种新的振动模式。这种新的振动模式依赖于内嵌旋转银纳米方块的旋转角度和边长。与没有嵌入银纳米方块和嵌入银纳米方块没有旋转时的金属-介质-金属波导滤波器相比,内嵌入旋转的银纳米方块的金属-介质-金属波导滤波器对周围介质折射率的微小变化更加敏感。因此,该结构在生物传感器方面具有潜在应用。

关键词:表面等离极化激元;金属-介质-金属波导;时域有限差分算法

中图分类号:O43 **文献标志码**:A **doi**:10.13883/j.issn1004-5929.201404014

Refractive Index Sensor Based on Circular Nanocavity Embedded with Tilted Silver Nanocube

CAO Wei [1], QIN Yan [1], ZHANG Zhong-yue [1,2*]

(1. *School of Physical Science and Technology, Southwest University, Chongqing* 400715, *China*;
2. *School of Physics and Information Technology, Shaanxi Normal University, Xi'an* 710062, *China*)

Abstract: A novel plasmonic sensor of circular nanocavity embedded with an Ag nanocube based on the metal-insulator-metal (MIM) waveguide was characterized by the finite-difference time-domain method. Since the tilted Ag nanocube breaks the symmetric steady-state magnetic field distribution, a new resonant mode occurs in the circular nanocavity. The resonance depends on the rotation angle and length of the cube. The MIM waveguide with a circular nanocavity embedded with a tilted Ag nanocube is more sensitive to small refractive index changes that fill the nanocavity than the MIM waveguide with a empty circular nanocavity and the MIM waveguide with circular nanocavity symmetrically embedded with an Ag nanocube. A potential application to biosensors has therefore been established.

Key words: Surface plasmon polaritons; metal-insulator-metal waveguide; finite-difference time-domain method

1 Introduction

Surface plasmon polaritons (SPPs) are electromagnetic waves that propagate in metals and dielectric interfaces[1]. SPPs have raised tremendous interest because of their emerging applications, such as in waveguides[2-4], metamaterials[5], data storages[6], and sensors[7]. Two basic types of SPP waveguides are widely investigated for waveguide application, insulator-metal-insulator (IMI) waveguide[8-10] and metal-insulator-metal (MIM) waveguide[11-17]. MIM waveguides have

收稿日期:2013-09-09;**修改稿日期**:2013-10-30
基金项目:国家自然科学基金资助的课题(11004160)
作者简介:曹威(1986-),男,硕士研究生,主研方向为微纳光学与光子学. E-mail: cw889126@126.com
通讯作者:张中月(1975-),男,教授,博士. E-mail: zyzhang@snnu.edu.cn

attracted substantial research attention because of their small mode size, and as a result, photonic devices based on MIM waveguides, such as filters[11-14], splitters[15-16], and couplers[17], have been realized.

In applying MIM waveguides to filters, the resonant wavelengths of the filter strongly depend on the refractive index of the filled media inside the cavity, this dependence enables changes in the refractive index to be detected[18-20]. Researchers have varied the topological shape of the nanocavity of the MIM waveguide to improve the sensitivity of sensors. For example, Zhang group proposed a plasmonic structure of the gear-shaped nanocavity. The gear breaks the symmetric distribution of the resonance to realize a new resonance and thus allows the sensitive detection of small refractive index changes compared with the MIM waveguide with a disk-shaped nanocavity[18]. Using the coupling between adjacent nanocavities, new resonance can also occur in the reflection spectra. For example, the research group of Liu proposed a system in a strongly confined MIM waveguide that is side-coupled with a pair of resonators, and the group achieved a sensitivity of approximately 900 nm / RIU [19].

This study shows that new resonance can be achieved in a circular nanocavity embedded with a tilted Ag nanocube of the MIM waveguide. The resonance strongly depends on the tilting angle and size of the Ag nanocube. The MIM waveguide with a circular nanocavity embedded with a tilted Ag nanocube is more sensitive to the small refractive index changes in the dielectric materials that fill the nanocavity than the MIM waveguide with an empty circular nanocavity and the MIM waveguide with a circular nanocavity symmetrically embedded with an Ag nanocube.

2　Structure and computational method

Fig. 1 shows the MIM waveguide with a circular nanocavity embedded with an Ag nanocube. The width w of the MIM waveguide is fixed at 50 nm to ensure that only the fundamental transverse magnetic mode is supported [20]. The cube has a length of L. The cube may rotate in the circular nanocavity. The rotation angle of the cube is defined as θ. In this study, we mainly investigated the effect of the cube on the resonance of the circular nanocavity. Some structural parameters of this composite structure are fixed, including the radius R of the circular nanocavity at 300 nm, the distance between the circular nanocavity and the MIM waveguide at 10 nm, and the thickness (in z-direction) of the structure at 600 nm. Perfectly matched layers are used around the proposed structure (in x- and y-directions). In z-direction, periodic boundaries are used.

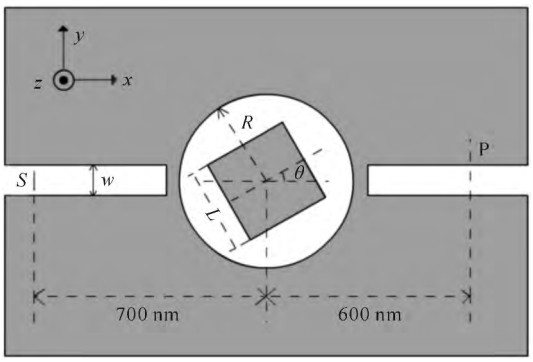

Fig. 1　Schematic structure of the circular nanocavity embedded with an Ag nanocube of the MIM waveguide with a slit width of w, a nanocavity radius of R, a cube length of L and the dipole excitation of S

The transmission properties of the MIM waveguide with a circular nanocavity embedded with an Ag nanocube are investigated with commercial finite-difference time-domain (FDTD) software (XFDTD by Remcom Inc.). The frequency-dependent complex relative permittivity of silver is characterized by the Drude model [21]. A dipole source S, which is in the middle of the waveguide at a distance of 700 nm away from the center of the circular nanocavity, oscillates as a Gaussian pulse with a pulse along the y-direction to excite the fundamental transverse magnetic mode in the MIM waveguide. The transmittance is determined as $T = P_T/P_0$, where P_T is the transmitted energy flow in the MIM waveguide

with a circular nanocavity embedded with a nanocube, and P_0 is the transmitted energy flow in the MIM waveguide without the nanocavity. The transmitted energy flow is determined by integrating the x-component of the Poynting vector over the cross section of the power monitors P at a distance of 1300 nm from the dipole source. The steady-state magnetic field distributions are calculated by using the excitation with a specific wavelength.

3 Results and discussion

3.1 simulation result and SPPs propagation mechanism

The transmission properties of the MIM waveguide with the circular nanocavity are also calculated to examine the effect of the embedded nanocube in the circular nanocavity on the transmission spectrum. Fig. 2(a) shows the transmission spectrum of the circular nanocavity. The radius of the circular nanocavity is $R = 300$ nm. Three obvious resonant modes (A_0, A_1 and A_2) appear in the transmission spectrum. When the nanocube is symmetrically embedded ($\theta = 0$) in the circular nanocavity, four resonant modes (B_0, B_1, B_2 and B_3) appear in the transmission spectrum, as shown in Fig. 2(b). Here the length of the nanocube is $L = 300$ nm. When the nancube tilted to $\theta = \pi/6$, the transmission spectrum is more complicate at shorter wavelength and five obvious resonant modes (C_0, C_1, C_2, C_3 and C_4) appear in the transmission spectrum, as shown in Fig. 2(c).

The normalized $|H_z|$ field distributions at the resonant wavelengths in Fig. 2 are calculated to further understand the nature of these wavelengths. Fig. 3(a-c) shows the normalized $|H_z|$ field distributions of the circular nanocavity at resonant wavelengths of $\lambda_{A0} = 0.716$ μm, $\lambda_{A1} = 0.546$ μm and $\lambda_{A2} = 0.448$ μm. Standing waves are formed inside the nanocavity. In Fig. 3(a), there are four parts with large magnetic fields inside the disk. Two of them correspond to transverse magnetic fields with the direction into the disk and two of them correspond to transverse magnetic fields with the direction out of the disk. Thus, there are two resonant wavelengths in the disk and the mode number is 2. Similarly, the mode numbers of A_1 and A_2 are 3 and 4, respectively. Fig. 3(d-f) shows the normalized $|H_z|$ field distributions of the circular nanocavity in which a nanocube is symmetrically embedded at resonant wavelengths of $\lambda_{B1} = 0.637$ μm, $\lambda_{B2} = 0.468$ μm, and $\lambda_{B3} = 0.431$ μm. As shown in Fig. 3(d), the $|H_z|$ field distribution is similar to that in Fig. 3(b) and the mode number is 3, which denotes the same resonant mode of the circular nanocavity at λ_{A1}. Similarly, the resonant modes at $\lambda_{B2} = 0.468$ μm (as shown in Fig. 3(e)) of the circular nanocavity symmetrically embedded with a nanocube is the same as that at $\lambda_{A2} = 0.448$ μm (as shown in Fig. 3(c)) of the circular nanocavity. As shown in Fig. 3(f), at $\lambda_{B3} = 0.431$ μm, ten parts with large magnetic fields appear in the nanocavity and the mode number is 5. Thus, when an Ag nanocube is symmetrically embedded in the circular nanocavity, new resonant mode oc-

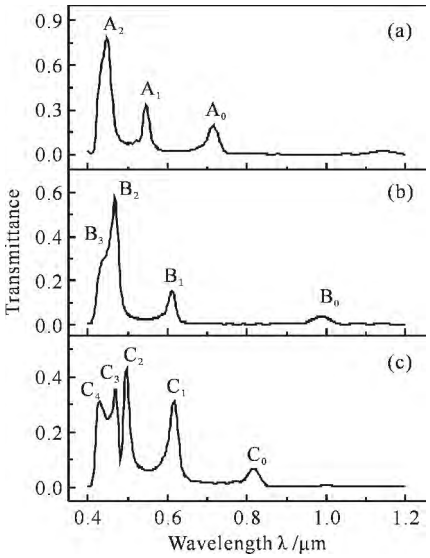

Fig. 2 Transmission spectra of the MIM waveguides with different Nanocavities. (a) the empty circular nanocavity; (b) the circular nanocavity embedded with an Ag nanocube at $\theta = 0$; (c) the circular nanocavity embedded with an Ag nanocube at $\theta = \pi/6$

curs in the transmission spectrum. At $\lambda_{B0}=0.988$ μm, the normal $|H_z|$ field distribution is similar to that in Fig. 3(a) and the mode number is 2 (not shown in Fig. 3). Fig. 3 (g-j) shows the normalized $|H_z|$ field distributions of the circular nanocavity embedded with a tilted Ag nanocube ($\theta=\pi/6$) at resonant wavelengths of $\lambda_{C0}=0.818$ μm, $\lambda_{C1}=0.616$ μm, $\lambda_{C2}=0.496$ μm and $\lambda_{C3}=0.468$ μm. In Fig. 3(g-i), there are similar magnetic field distributions as those in Fig. 3(a-c), which denotes the same mode number of 2, 3 and 4, respectively. However, Fig. 3(j) shows that distinguishing the mode number in the $|H_z|$ fields distribution is difficult at $\lambda_{C3}=0.468$ μm. This transmission peak is a novel resonant mode when the nanocube is tilted inside the circular nanocavity. For the circular nanocavity embedded with a tilted nanocube, the nanocube breaks the symmetry of the $|H_z|$ field distribution of the circular nanocaivty and thus forms the novel resonant mode in the transmission spectrum. This phenomenon can also be explained by the resonance from the interference between the discrete resonance of the tilting nanocube and the symmetric distribution of the resonance in the circular nanocavity.

3.2　Structure parameters influence

θ is increased from $\theta=0$ to $\theta=\pi/4$ at a fixed $L=300$ nm and $R=300$ nm to investigate how the tilting angle θ affects the resonance. Fig. 4 shows that θ slightly shifts the resonant modes. However, the intensity of the transmittance at the resonant wavelength strongly depends on θ. When $\theta=0$, a broad band appears from 0.4 μm to 0.5 μm in the transmission spectrum. The resonant mode of C_2 becomes increasingly clear and reaches its maximum at $\theta=\pi/9$ as θ increases. The transmittance at C_2 decreases as θ further increases. The changes of the transmittance are due to the steady-state magnetic field distribution relative to the waveguide from which SPPs are coupled out of the nanocavity. Similarly, the resonant modes of C_3 and C_4 also strongly depend on θ. The rotating angle of the nanocube strongly affects the distribution of the steady-state electric field relative to the coupling end of the MIM waveguide, which results in the strongly θ-dependent resonant modes in Fig. 4.

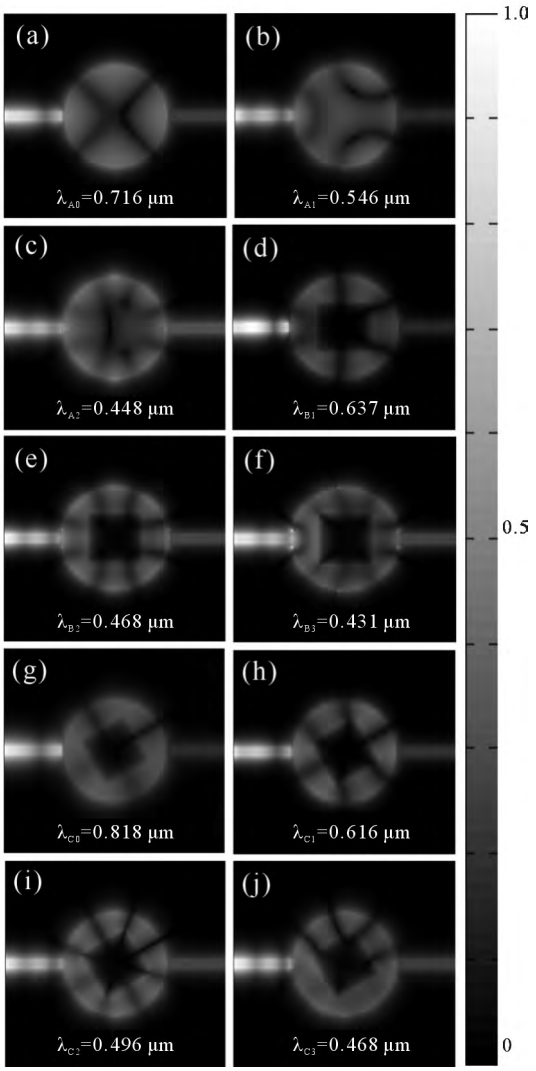

Fig. 3　Contour profiles of the normalized $|H_z|$ fields distributions of the MIM waveguide with different nanocavities and wavelengths. (a-c) the empty circular nanocavity at resonant wavelengthes of 0.716 μm, 0.546 μm and 0.448 μm, respectively; (d-f) the circular nanocavity embedded with and Ag nanocube ($\theta=0$) at resonant wavelengths of 0.637 μm, 0.468 μm and 0.431 μm, respectively; (g-j) the circularnanocavity embedded with the Ag nanocube ($\theta=\pi/6$) at resonant wavelengthes of 0.818 μm, 0.616 μm, 0.496 μm and 0.468 μm, respectively

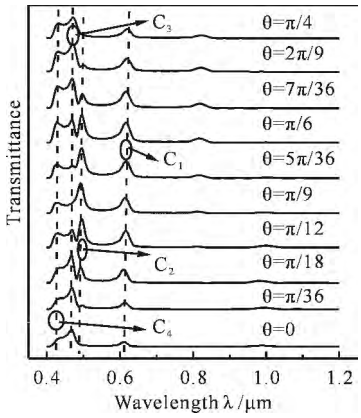

Fig. 4 Transmission spectra of the MIM waveguide with an Ag nanocube embedding the circular nanocavity with various rotation angle of θ at cube length $L=300$ nm

L is increased from $L=220$ nm to $L=380$ nm at fixed $\theta=\pi/6$ to investigate the effect of nanocube length L on the resonance in the circular nanocavity embedded with a tilted nanocube. Fig. 5 shows that three resonant modes ($\lambda=0.756$ μm, 0.562 μm, and 0.454 μm) red shift in the transmission spectrum at $L=220$ nm compared with those of the circular nanocavity. The resonant modes red shift monotonically as L increases, and the resonant mode at $\lambda=0.468$ μm splits. Three obvious resonant modes can be observed when $L=220$ nm and $L=260$ nm. When $L=300$ nm and $L=340$ nm, five resonant modes can be observed. When $L=380$ nm, six obvious resonant modes appear. Electric field coupling between the nanocube and the inner surface of the nanocavity is relatively weak with smaller L. Therefore, the embedded nanocube does not produce a new resonant mode and only makes the resonant modes red shift. However, this electric field coupling becomes strong with a large L. The embedded nanocube does not only make the resonant modes red shift but also forms new resonant modes at the blue side of the transmission spectrum.

3.3 Applications

We compared the sensitivity to the refractive index of the filled media of the circular nanocavity with those of the filled media of the circular nanocavity embedded with an Ag nanocube to test

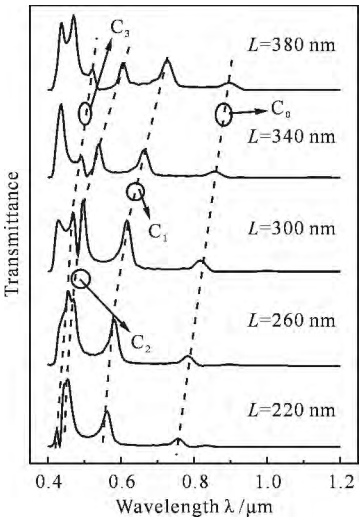

Fig. 5 (Color online) Transmission spectra of the MIM waveguide with an Ag nanocube embedding the circular nanocavity with various cube length of L at rotation angle of $\theta=\pi/6$

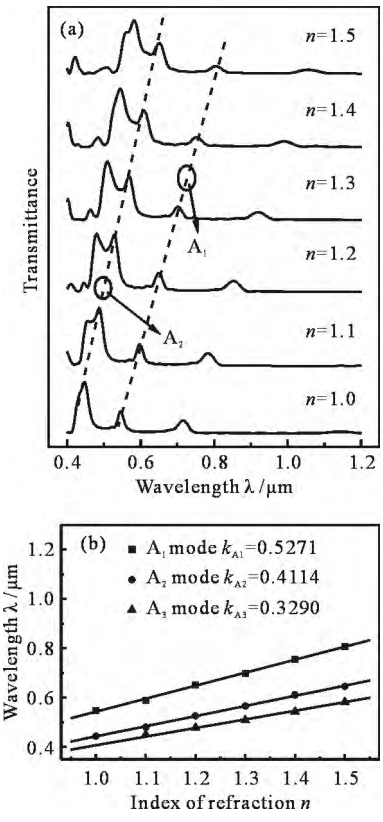

Fig. 6 (a) Transmission spectra of the MIM waveguide with the empty circular nanocavity filled by different refractive index n; (b) Resonant wavelengths as a function of the refractive index n

whether the embedded nanocube contributes to the sensitivity of the resonant modes. The circular nanocavities have the same radius, $R = 300$ nm. Fig. 6(a) shows the transmission spectra of the empty circular nanocavity with different filled refractive index n. The wavelengths of the resonant modes red shift as n increases, and new resonant modes appear at the blue side of the transmission spectra. Fig. 6(b) display the wavelengths of the A_1, A_2 and A_3 modes as a function of refractive index n. The solid curves are the results of linear fitting. The slopes of the solid curves shown in Fig. 6(b) are $k_{A1} = 0.5271$, $k_{A2} = 0.4114$ and $k_{A3} = 0.3290$, respectively. Fig. 7(a) shows the transmission spectra of the circular nanocavity symmetrically embedded with an Ag nanocube with different filled refractive index n. The wavelengths of the resonant modes red shift as n increases. Fig. 7(b) display the wavelengths of the B_1, B_2 and B_3 modes as a function of refractive index n. The solid curves are the results of linear fitting. The slopes of them are $k_{B1} = 0.5798$, $k_{B2} = 0.4323$ and $k_{B3} = 0.3136$, respectively. Fig. 8(a) shows the transmission spectra of the circular nanocavity embedded with a tilted Ag nanocube ($\theta = \pi/6$) with different filled refractive index n. Fig. 8(b) display the wavelengths of the C_1, C_2 and C_3 modes as a function of refractive index n. The solid curves are the results of linear fitting. The slopes of them are $k_{C1} = 0.5923$, $k_{C2} = 0.4560$ and $k_{C3} = 0.4314$, respectively. It is found that $k_{C1} > k_{B1} > k_{A1}$, $k_{C2} > k_{B2} > k_{A2}$, $k_{C3} > k_{A3} > k_{B3}$. Thus, the resonant modes are sensitive to the refractive index when the tilted Ag nanocube is embedded in the circular nanocavity. A sensitive method to detect changes in the refractive index has therefore been developed.

4　Conclusions

A novel plasmonic MIM waveguide sensor of a circular nanocavity embedded with an Ag nanocube is proposed in this study. The transmission properties of the proposed waveguide filter are investigated by the FDTD method and compared with those of a circular nanocavity without an embedded nanocube. The tilting nanocube breaks the symmetric distribution of the resonant modes of the circular nanocavity to realize new resonance. The resonant modes of the circular nanocavity embedded with tilted Ag nanocube are sensitive to the small changes in refractive index of the materials that fill the nanocavity. A potential application to biosensors has therefore been established.

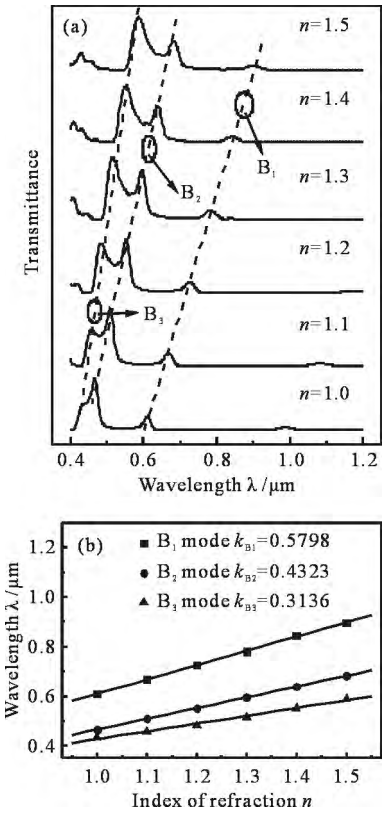

Fig. 7　(a) Transmission spectra of the MIM waveguide with an Ag nanocube embedding the circular nanocavity ($\theta = 0$) filled by different refractive index n; (b) Resonant wavelengths as a function of the refractive index n

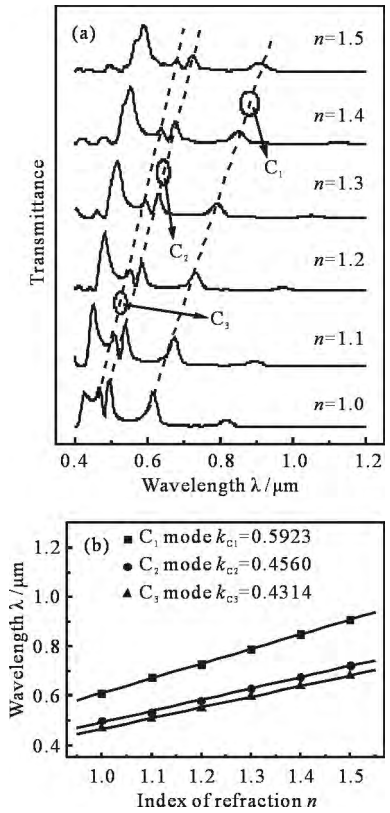

Fig. 8 (a) Transmission spectra of the MIM waveguide with an Ag nanocube embedding the circular nanocavity ($\theta = \pi/6$) filled by different refractive index n; (b) Resonant wavelengths as a function of the refractive index n

References:

[1] Bozhevolnyi S I, Volkov V S, Devaux E, *et al*. Channel plasmon subwavelength waveguide components including interferometers and ring resonators [J]. Nature, 2006, 440:508-511.

[2] Gramotnev D K, Bozhevolnyi S I. Plasmonics beyond the diffraction limit[J]. Nat Photonics 2010,4: 83-91.

[3] Xue W R, Guo Y N, Zhang W M. Propagation properties of a modified surface plasmonic waveguide with an arc slot[J]. Chin Phys B, 2009, 18(6):2529-2534.

[4] Liu B C, Yu L, Lu Z X. The surface plasmon polariton dispersion relations in a nonlinear-metal-nonlinear dielectric structure of arbitrary nonlinearity [J]. Chin Phys B, 2011,20(3):037302-6.

[5] Caloz C. Perspectives on EM metamaterials [J]. Mate. Today 2009,12(3):12-206.

[6] Chen W T, Wu P C, Chen C J, *et al*. Manipulation of multidimensional plasmonic spectra for information storage[J]. Appl Phys Lett, 2011, 98(17): 171106-8.

[7] Charbonneau R, Tencer M, Lahoud N, *et al*. Demonstration of surface sensing using long-range surface plasmon waveguides on silica[J]. Sensor Actuat B-Chem, 2008,134:455-461.

[8] Fang Y R, Li Z P, Huang Y Z, *et al*. Branched Silver Nanowires as Controllable Plasmon Routers[J]. Nano Lett, 2010,10:1950-1954.

[9] Wang W, Yang Q, Fan F, *et al*. Light Propagation in Curved Silver Nanowire Plasmonic Waveguides [J]. Nano Lett, 2011,11:1603-1608.

[10] Krasavin A V, Zayats A V. Guiding light at the nanoscale: numerical optimization of ultrasubwavelength metallic wire plasmonic waveguides[J]. Opt Lett, 2011,36(16):3127-3129.

[11] Lin X S, Huang X G. Tooth-shaped plasmonic waveguide filters with nanometeric sizes[J]. Opt Lett, 2008,33(23):2874-2876.

[12] Setayesh A, Mirnaziry S R, Abrishamian M S. Numerical investigation of a tunable band-pass plasmonic filters with a hollow-core ring resonator[J]. J Opt, 2011,13:035004-7.

[13] Zhu J H, Wang Q J, Shum P, *et al*. A Nanoplasmonic High-PassWavelength Filter Based on a Metal-Insulator-Metal Circuitous Waveguide[J]. IEEE T Nanotechnol, 2011,10(6):1357-1361.

[14] Yun B, Hu G, Cui Y. Theoretical analysis of a nanoscale plasmonic Filter based on a rectangular metal-insulator-metal waveguide [J]. J Phys D, 2010,43:385102-8.

[15] Chen J J, Li Z, Lei M, *et al*. Plasmonic Y-splitters of High Wavelength Resolution Based on Strongly Coupled-Resonator Effects[J]. Plasmonics,2012,7: 441-445.

[16] Reiserer A A, Huang J S, Hecht B, *et al*. Plasmonic Y-splitters of High Wavelength Resolution Based on Strongly Coupled-Resonator Effects[J]. Opt Express, 2010,18(11):11810-11820.

[17] Zenin V A, Volkov V S, Han Z H, *et al*. Directional coupling in channel plasmon-polariton waveguides[J]. Opt Express, 2012,20(6):6124-6134.

[18] Zhang Z D, Wang H Y, Zhang Z Y. Fano Resonance in a Gear-Shaped Nanocavity of the Metal-In-

sulator-Metal Waveguide [J]. Plasmonics, 2012,8: 797-801.

[19] Lu H, Liu X M, Mao D, *et al*. Plasmonic nanosensor based on Fano resonance in waveguide-coupled resonators [J]. Opt Lett, 2012,37(18):3780-3782.

[20] Kekatpure R D, Hryciw A C, Barnard E S, *et al*. Solving dielectric and plasmonic waveguide dispersion relations on a pocket calculator[J]. Opt Express, 2009,17(26):24112-24129.

[21] Gai H F, Wang J, Tian Q. Modified Debye model parameters of metals applicable for broadband calculations[J]. Appl Opt, 2007,46(12):2229-2233.